Bifunctional Zeolite based Catalysts and Innovative process for Sustainable Hydrocarbon Transformation

BiZeolCat

Dehydrogenations multi-scale process modelling

Blaž Likozar, Drejc Kopač, Damjan Lašič Jurković, Matej Huš

National Institute of Chemistry, Slovenia

Joint Webinar, April 13, 2021

This project has received funding from the European Union's Horizon 2020 research and innovation programme under grant agreement No 814671.

The present publication reflects only the author's views and the European Union is not liable for any use that may be made of the information contained therein.

(*Disclosure or reproduction without prior permission of BIZEOLCAT is prohibited).*

Propane dehydrogenation

CATOFIN® process

- chromia catalysts alumina support
- 850 K
- 1.2-1.5 bar O_2
- <70% conversion

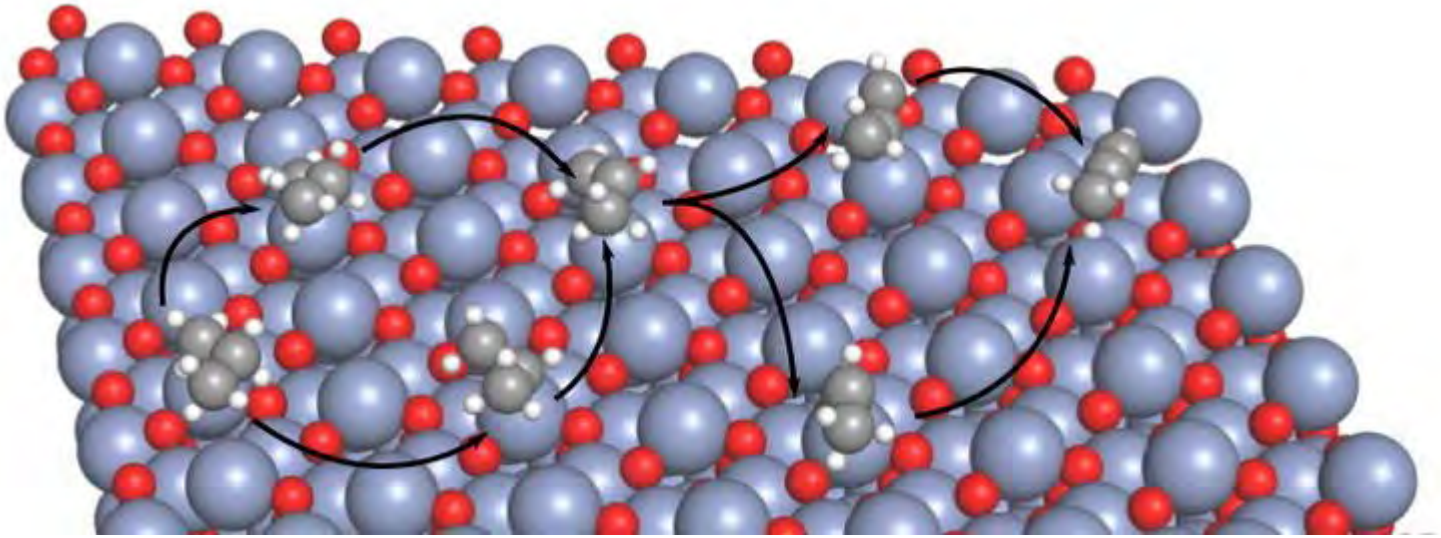

This project has received funding from the European Union's Horizon 2020 research and innovation program under grant agreement no 814671

BiZeolCat

Atomistic level

Methods:

- **Electronic level:** Density functional theory (DFT) calculations
  - Perdew-Wang 91 functional (GGA)
  - DFT+U for the *3d* states of Cr, *D-J* = 4 eV
  - The Grimme dispersion (D3) correction
- **Surface level:** Kinetic Monte Carlo modelling
  - A 25 x 25 lattice with two **four** types of active sites (oxidised and reduced surface)
  - Using DFT calculated kinetic and TD parameters, 10^7 events
- **Meso- and macroscopic:** Kinetic modelling (ODEs)

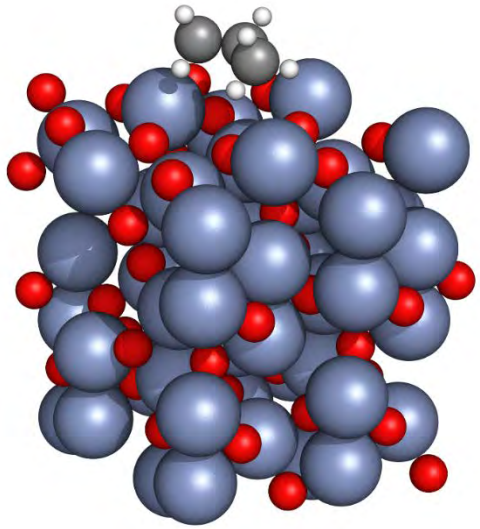

Model:

- Based on the CATOFIN® process (chromia catalysts, alumina support, 850 K, 1.2-1.5 bar O_2, <70% conversion)
- Bulk α-Cr_2O_3 cut along the (0001) surface
- Cr termination – reduced surface, O termination – oxidised surface
- Added dopants to the surface
- 12 alternating layers (6 for O, 6 Cr)
- A 2x2 supercell (2*a* = 10.18 Å)
- Vacuum in the *z* direction: 15 Å, dipole correction included

This project has received funding from the European Union's Horizon 2020 research and innovation program under grant agreement no 814671

Oxidation state of the surface

Reduced vs. oxidised surface

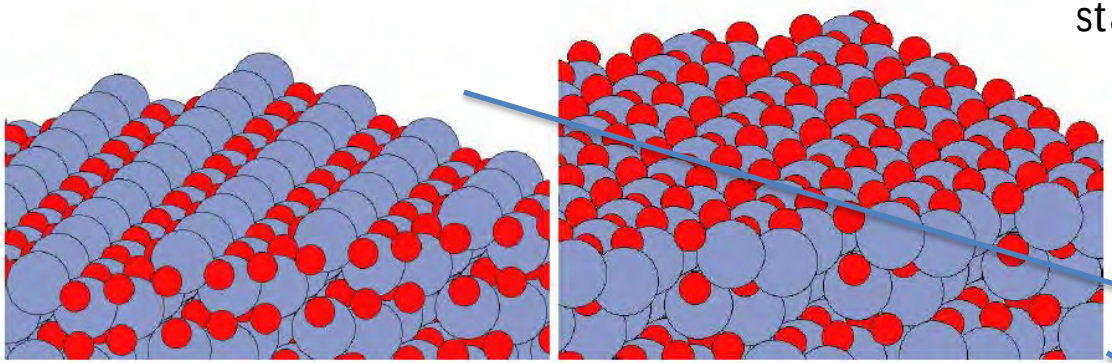

Left: reduced surface (Cr- terminated), right: oxidised surface (O-terminated)

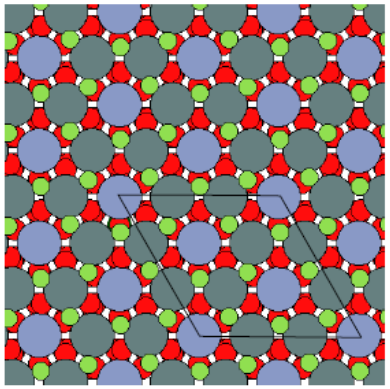

Top view of the oxidised surface. For the reduced surface, an additional layer of Cr atoms is situated atop. Colour code: red - O, blue - Cr, green - O (top), teal - Cr (top).

Reduced surface

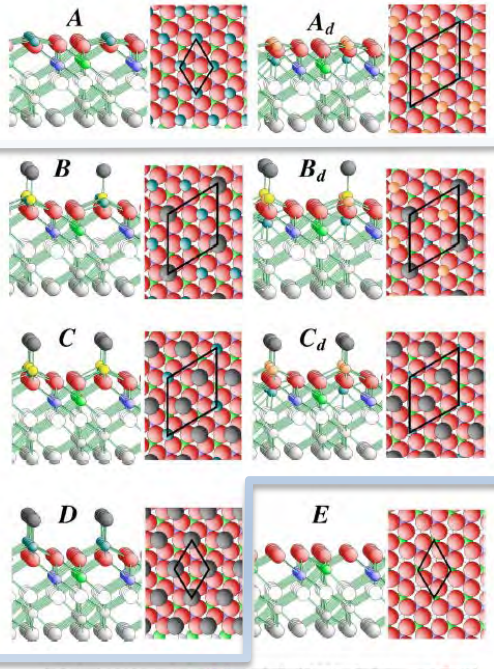

Intermediate oxidation states

Oxidised

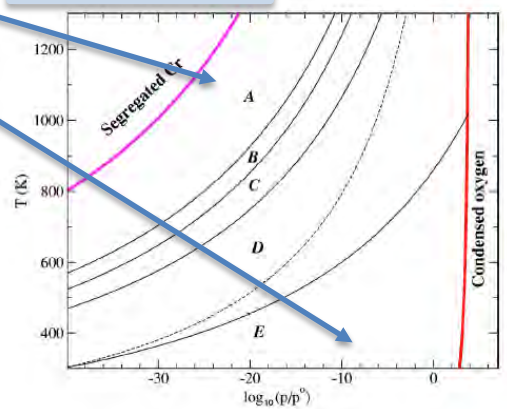

Wang X.-G. and Smith, J. R. Surface phase diagram for Cr_2O_3(0001): Ab initio density functional study. *Physical Review B*, 68, 201402, **2003**.

This project has received funding from the European Union's Horizon 2020 research and innovation program under grant agreement no 814671

Interconversion between the reduced and oxidised surface

On the oxidised surface, **MvK** is possible. Two adjacent H* form H_2O* with a surface lattice oxygen atom, which can desorb, yielding an oxygen vacancy (reduced surface). The ensuing vacancy can be replenished with CO_2 (unfavourable), N_2O (possible) or O_2 (when two are adjacent). W/o an oxidant, the surface gets reduced. **Included in the model.**

	reaction	E_A (eV)	ΔE (eV)¶
1	$2\ H^* \rightarrow H_2O^*_{surf} + *$	1.19	+0.91
2	$H_2O^*_{surf} \rightarrow H_2O(g) + V^*$	1.36	+1.36
3	$V^* + * \rightarrow * + V^*$	0.63	+0.00
4	$V^* + N_2O(g) \rightarrow * + N_2(g)$	0.73	−1.32
5	$V^* + CO_2(g) \rightarrow * + CO(g)$	2.73	+2.35
6	$2\ V^* + O_2(g) \rightarrow O_2^{V^*}$	0.00	−0.89
7	$O_2^{V^*} \rightarrow 2\ *$	0.64	−1.41

2 H* recombine into H_2O* on the ox. surf. H_2O desorption yielding the red. surf.

Replenishment with N_2O

Replenishment with CO_2

Replenishment with O_2 (two steps)

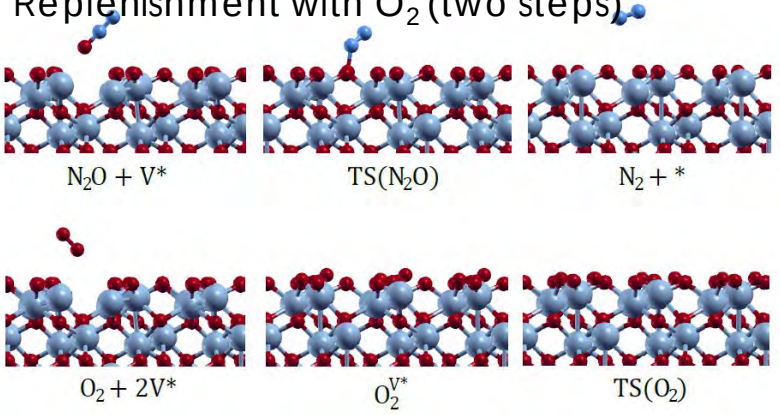

Net reactions differ when oxidants are used.

$C_3H_8 \rightarrow CH_3CH{=}CH_2 + H_2$

$C_3H_8 \rightarrow CH_3C{\equiv}CH + 2\ H_2$

$C_3H_8 + ½O_2 \rightarrow CH_3CH{=}CH_2 + H_2O$

$C_3H_8 + O_2 \rightarrow CH_3C{\equiv}CH + 2\ H_2O$

This project has received funding from the European Union's Horizon research and innovation program under grant agreement no 81467

Adsorption

species	Reduced surface (A)				Oxidised surface (E)			
	$E_{surf,dis}$	E_{dis}	E_{int}	E_{ads}	$E_{surf,dis}$	E_{dis}	E_{int}	E_{ads}
C_3H_8	0.00	0.02	−0.38	**−0.36**	0.01	0.01	−0.25	**−0.23**
$CH_3CH{=}CH_2$	0.03	0.02	−0.50	**−0.45**	1.20	2.68	−6.88	**−3.00**
$CH_3C{\equiv}CH$	0.04	0.02	−0.69	**−0.63**	3.40	3.59	−11.09	**−4.10**
C_2H_6	0.00	0.02	−0.25	**−0.23**	0.00	0.00	−0.21	**−0.21**
$CH_2{=}CH_2$	0.02	0.02	−0.43	**−0.39**	1.16	2.45	−6.50	**−2.89**
$CH{\equiv}CH$	0.04	0.02	−0.46	**−0.40**	2.78	3.26	−10.23	**−4.19**
CH_4	0.00	0.01	−0.15	**−0.14**	0.00	0.00	−0.11	**−0.11**
H_2	0.00	0.00	−0.04	**−0.04**	0.00	0.00	0.00	**0.00**

- Propane, ethane, methane adsorb negligibly
- CH_x with double and triple bonds adsorb **moderately** on the **reduced surface** and **extremely strongly** on the **oxidised surface**
- **Oxidised surface** expected to be more active towards dehydrogenation and cracking

Surface distortion (unfavourable)

Distortion effect (unfavourable)

Electronic effect (favourable)

Total adsorption interaction

This project has received funding from the European Union's Horizon 2020 research and innovation program under grant agreement no 814671

Reaction mechanism

Reaction mechanism:

- Two types of elementary reactions:
  - dehydrogenations (C-H bond) and
  - cracking (C-C bond).

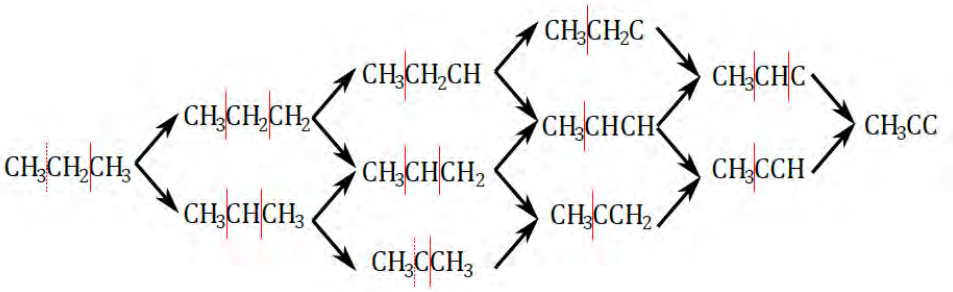

Vector space for possible elementary reactions the same on the oxidised and reduced surface.

Reactions that actually happen differ between the surfaces.

All possible reaction steps were calculated on both surfaces.

They are to be used for modelling the effect of the oxidation state.

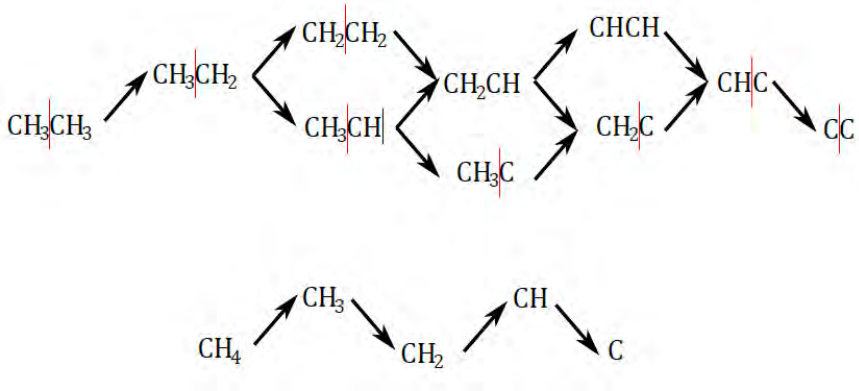

This project has received funding from the European Union's Horizon 2020 research and innovation program under grant agreement no 814671

Reaction mechanism

- Adsorptions of non-saturated CH_x much stronger
- Greater affinity for hydrogen on the oxidised surface, similar activation barrier
- Lower mobility of H on the oxidised surface (strongly bound)

	reaction step	type	Reduced surface (A) E_A	Reduced surface (A) ΔE ¶	Oxidised surface (E) E_A	Oxidised surface (E) ΔE ¶
8&	$H_2(g) + 2\# \rightarrow H_2{}^{\#\#}$	ads.	0	−0.04	0	0.00
9&	$C_3H_8(g) + * \rightarrow C_3H_8{}^*$	ads.	0	−0.37	0	−0.23
10&	$CH_3CH{=}CH_2(g) + * \rightarrow CH_3CHCH_2{}^*$	ads.	0	−0.45	0	−3.00
11&	$CH_3C{\equiv}CH(g) + * \rightarrow CH_3CCH^*$	ads.	0	−0.61	0	−4.10
12&	$CH_3CH_3(g) + * \rightarrow CH_3CH_3{}^*$	ads.	0	−0.23	0	−0.21
13&	$CH_2{=}CH_2(g) + * \rightarrow CH_2CH_2{}^*$	ads.	0	−0.39	0	−2.89
14&	$CH{\equiv}CH(g) + * \rightarrow CHCH^*$	ads.	0	−0.40	0	−4.19
15&	$CH_4(g) + * \rightarrow CH_4{}^*$	ads.	0	−0.14	0	−0.11
16	$H_2{}^{\#\#} \rightarrow 2\,H^{\#}$	dis.	0.54	−0.83	0.58	−3.40
17&	$H^{\#} + \# \rightarrow \# + H^{\#}$	diff.	0.61	0	0.94	0

This project has received funding from the European Union's Horizon 2020 research and innovation program under grant agreement no 814671

BiZeolCat

Reaction mechanism

- Reaction endothermic on the reduced surface and exothermic on the oxidised surface
- Lower barriers on the oxidised surface

	reaction step	type	Reduced surface (A) E_A	Reduced surface (A) ΔE ¶	Oxidised surface (E) E_A	Oxidised surface (E) ΔE ¶
18	$C_3H_8{}^* + \# \rightarrow CH_3CH_2CH_2{}^* + H^\#$	dehydr.	1.25	+0.85	0.19	−2.64
19	$C_3H_8{}^* + \# \rightarrow CH_3CHCH_3{}^* + H^\#$	dehydr.	1.27	+0.73	0.11	−2.70
20	$CH_3CH_2CH_2{}^* + \# \rightarrow CH_3CH_2CH^* + H^\#$	deep	1.88	+1.59	0.55	−1.88
21	$CH_3CH_2CH_2{}^* + \# \rightarrow CH_3CHCH_2{}^* + H^\#$	dehydr.	1.37	+0.04	1.76	−2.27
22	$CH_3CHCH_3{}^* + \# \rightarrow CH_3CHCH_2{}^* + H^\#$	dehydr.	0.84	+0.16	0.69	−2.21
23	$CH_3CHCH_3{}^* + \# \rightarrow CH_3CCH_3{}^* + H^\#$	deep	1.74	+1.44	3.57	−2.08
24	$CH_3CH_2CH^* + \# \rightarrow CH_3CH_2C^* + H^\#$	deep	1.87	+1.62	0.60	+0.45
25	$CH_3CH_2CH^* + \# \rightarrow CH_3CHCH^* + H^\#$	deep	1.79	−0.64	0.21	−2.16
26	$CH_3CHCH_2{}^* + \# \rightarrow CH_3CHCH^* + H^\#$	dehydr.	1.42	+0.90	2.14	−1.77
27	$CH_3CHCH_2{}^* + \# \rightarrow CH_3CCH_2{}^* + H^\#$	dehydr.	1.22	+0.82	0.23	−1.90
28	$CH_3CCH_3{}^* + \# \rightarrow CH_3CCH_2{}^* + H^\#$	deep	0.64	−0.46	0.20	−2.03
29	$CH_3CH_2C^* + \# \rightarrow CH_3CHC^* + H^\#$	deep	0.30	−0.59	0.21	−2.34
30	$CH_3CHCH^* + \# \rightarrow CH_3CHC^* + H^\#$	deep	1.98	+1.68	2.40	+0.27
31	$CH_3CHCH^* + \# \rightarrow CH_3CCH^* + H^\#$	dehydr.	1.81	+0.37	0.96	−0.99
32	$CH_3CCH_2{}^* + \# \rightarrow CH_3CCH^* + H^\#$	dehydr.	1.31	+0.45	0.83	−0.86
33	$CH_3CHC^* + \# \rightarrow CH_3CC^* + H^\#$	deep	0.86	−0.62	0.35	−0.90
34	$CH_3CCH^* + \# \rightarrow CH_3CC^* + H^\#$	deep	0.92	+0.69	0.95	−0.36

This project has received funding from the European Union's Horizon 2020 research and innovation program under grant agreement no 814671

BiZeolCat

Reaction mechanism

- Cracking strongly endothermic on the reduced surface, moderately exothermic on the oxidised surface
- On average, lower barriers on the oxidised surface
- Only steps with Ea < 3.5 eV shown. Different cracking routes on the surfaces.

	reaction step	type	Reduced surface (A) E_A	Reduced surface (A) ΔE ¶	Oxidised surface (E) E_A	Oxidised surface (E) ΔE ¶
35	$C_3H_8{}^* + * \rightarrow CH_3CH_2{}^* + CH_3{}^*$	cracking	3.23	+1.23	3.02	−2.41
36	$CH_3CH_2CH_2{}^* + * \rightarrow CH_3CH_2{}^* + CH_2{}^*$	cracking	2.90	+1.92	1.96	−1.11
37	$CH_3CH_2CH_2{}^* + * \rightarrow CH_3{}^* + CH_2CH_2{}^*$	cracking	2.32	+0.60	3.15	−1.79
38	$CH_3CHCH_3{}^* + * \rightarrow CH_3CH^* + CH_3{}^*$	cracking	2.95	+2.22	1.83	−1.58
39	$CH_3CHCH_2{}^* + * \rightarrow CH_3{}^* + CH_2CH^*$	cracking	3.29	+1.44	1.96	−1.28
40	$CH_3CHCH_2{}^* + * \rightarrow CH_3CH^* + CH_2{}^*$	cracking	N/A	N/A	0.92	−0.71
41	$CH_3CCH_3{}^* + * \rightarrow CH_3C^* + CH_3{}^*$	cracking	2.55	+2.16	N/A	N/A
42	$CH_3CH_2CH^* + * \rightarrow CH_3{}^* + CH_2CH^*$	cracking	3.20	−0.11	2.81	−1.67
43	$CH_3CHCH^* + * \rightarrow CH_3{}^* + CHCH^*$	cracking	2.79	+1.26	2.30	−0.52
44	$CH_3CCH_2{}^* + * \rightarrow CH_3{}^* + CH_2C^*$	cracking	3.03	+2.24	N/A	N/A
45	$CH_3CH_2C^* + * \rightarrow CH_3{}^* + CH_2C^*$	cracking	2.76	−0.11	1.64	−1.76
46	$CH_3CCH^* + * \rightarrow CH_3{}^* + CHC^*$	cracking	3.14	+1.46	N/A	N/A
47	$CH_3CHC^* + * \rightarrow CH_3{}^* + CHC^*$	cracking	3.13	+0.16	2.66	−0.29
48	$CH_3CHC^* + * \rightarrow CH_3CH^* + C^*$	cracking	N/A	N/A	0.70	+0.22

This project has received funding from the European Union's Horizon 2020 research and innovation program under grant agreement no 814671

Reaction mechanism

	reaction step	type	Reduced surface (A)		Oxidised surface (E)	
			E_A	ΔE ¶	E_A	ΔE ¶
49	$C_2H_6{}^* + \# \rightarrow CH_3CH_2{}^* + H^\#$	dehydr.	1.42	+0.76	0.28	−2.66
50	$CH_3CH_2{}^* + \# \rightarrow CH_2CH_2{}^* + H^\#$	dehydr.	1.42	+0.21	0.92	−2.01
51	$CH_3CH_2{}^* + \# \rightarrow CH_3CH^* + H^\#$	deep	1.99	+1.72	0.43	−1.87
52	$CH_2CH_2{}^* + \# \rightarrow CH_2CH^* + H^\#$	dehydr.	1.28	+0.88	0.36	−1.77
53	$CH_3CH^* + \# \rightarrow CH_3C^* + H^\#$	deep	1.59	+1.83	0.64	+0.39
54	$CH_3CH^* + \# \rightarrow CH_2CH^* + H^\#$	deep	0.60	−0.63	0.13	−1.91
55	$CH_2CH^* + \# \rightarrow CH_2C^* + H^\#$	deep	1.86	+1.63	1.33	+0.36
56	$CH_2CH^* + \# \rightarrow CHCH^* + H^\#$	dehydr.	1.47	+0.72	0.13	−1.01
57	$CH_3C^* + \# \rightarrow CH_2C^* + H^\#$	deep	0.17	−0.83	0.04	−1.94
58	$CHCH^* + \# \rightarrow CHC^* + H^\#$	deep	0.70	+0.58	1.10	+0.51
59	$CH_2C^* + \# \rightarrow CHC^* + H^\#$	deep	0.55	−0.32	0.26	−0.69
60	$CHC^* + \# \rightarrow CC^* + H^\#$	deep	1.99	+3.04	1.07	+0.92
61	$C_2H_6{}^* + * \rightarrow CH_3{}^* + CH_3{}^*$	cracking	3.13	+1.11	2.81	−2.23
62	$CH_3CH_2{}^* + * \rightarrow CH_3{}^* + CH_2{}^*$	cracking	2.75	+1.89	2.25	−0.91
63	$CH_2CH_2{}^* + * \rightarrow CH_2{}^* + CH_2{}^*$	cracking	N/A	N/A	1.05	−0.23
64	$CH_3CH^* + * \rightarrow CH_3{}^* + CH^*$	cracking	2.53	+2.27	N/A	N/A
65	$CH_3C^* + * \rightarrow CH_3{}^* + C^*$	cracking	2.30	+2.03	1.59	−1.30
66	$CH_2C^* + * \rightarrow CH_2{}^* + C^*$	cracking	N/A	N/A	0.26	−0.69
67	$CHC^* + * \rightarrow CH^* + C^*$	cracking	N/A	N/A	1.12	+0.66
68	$CC^* + * \rightarrow C^* + C^*$	cracking	N/A	N/A	0.45	−2.61
69	$CH_4{}^* + \# \rightarrow CH_3{}^* + H^\#$	deep	1.42	+0.78	0.48	−2.46
70	$CH_3{}^* + \# \rightarrow CH_2{}^* + H^\#$	deep	1.98	+1.54	0.64	−1.34
71	$CH_2{}^* + \# \rightarrow CH^* + H^\#$	deep	2.31	+2.11	0.69	+0.48
72	$CH^* + \# \rightarrow C^* + H^\#$	deep	1.86	+2.01	1.09	−2.35

This project has received funding from the European Union's Horizon 2020 research and innovation program under grant agreement no 814671

Effect of oxidant

- Potential energy surface calculated (also ΔG but not shown here)
- Two surfaces: oxidised (red) and reduced (black)
- On the oxidised surface, the reaction is exothermic. On the reduced, endothermic.
- Cracking not shown (calculated).
- Included MvK interconversion of the surfaces.
- Included burning away surface deposits of C* (due to coking) with excess O_2 and surface oxygen O*.

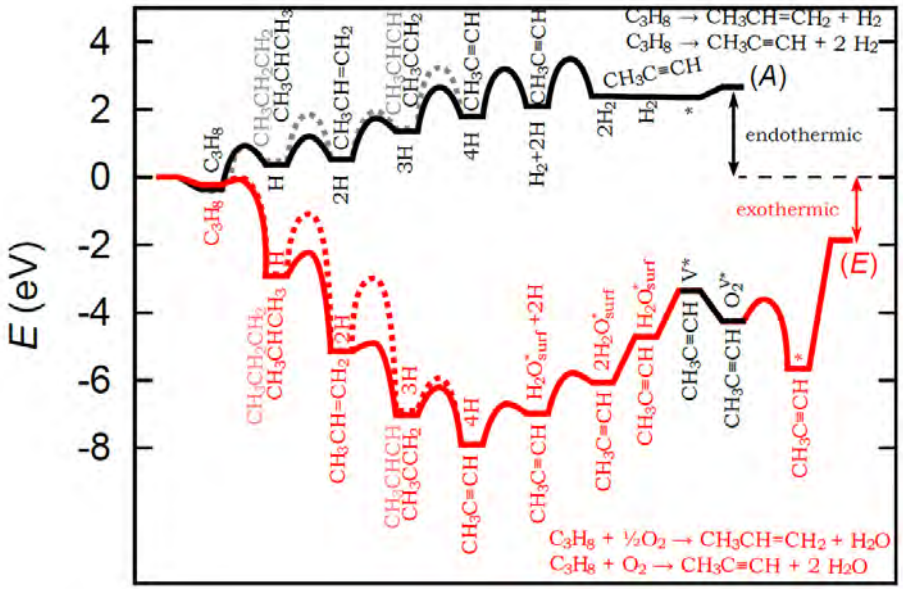

This project has received funding from the European Union's Horizon 2020 research and innovation program under grant agreement no 814671

Effect of surface oxidation

Methods (KMC):

- A graph-theoretical approach (ZACROS), stiffness scaling of fast steps (adsorptions, diffusion)
- Rate expressions calculated via the TST from DFT data
- Including the ZPE and Gibbs free energy contributions (in the harmonic approximation)
- LH, ER and non-activated reaction steps, surface interconversion (oxidised, reduced)
- Effect of oxidants used (CO_2, N_2O, O_2)

Model (KMC):

- A quasi-hexagonal lattice with four types of active sites ($O_{reduced}$, $Cr_{reduced}$, $O_{oxidised}$, $Cr_{oxidised}$,) – see on the right
- In total 324 sites
- Initially clear lattice
- 10^7 events
- Varying the operating conditions:
  - *Pressure*
  - *Temperature*
  - *Influx mixture composition*
  - *Oxidant used*
  - *Oxidation state of the surface (ratio)*

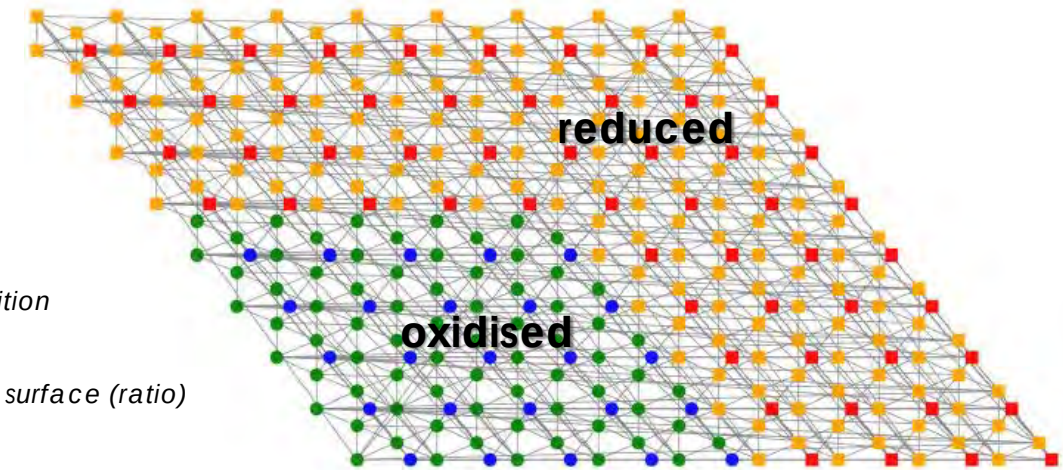

This project has received funding from the European Union's Horizon 2020 research and innovation program under grant agreement no 814671

Effect of surface oxidation

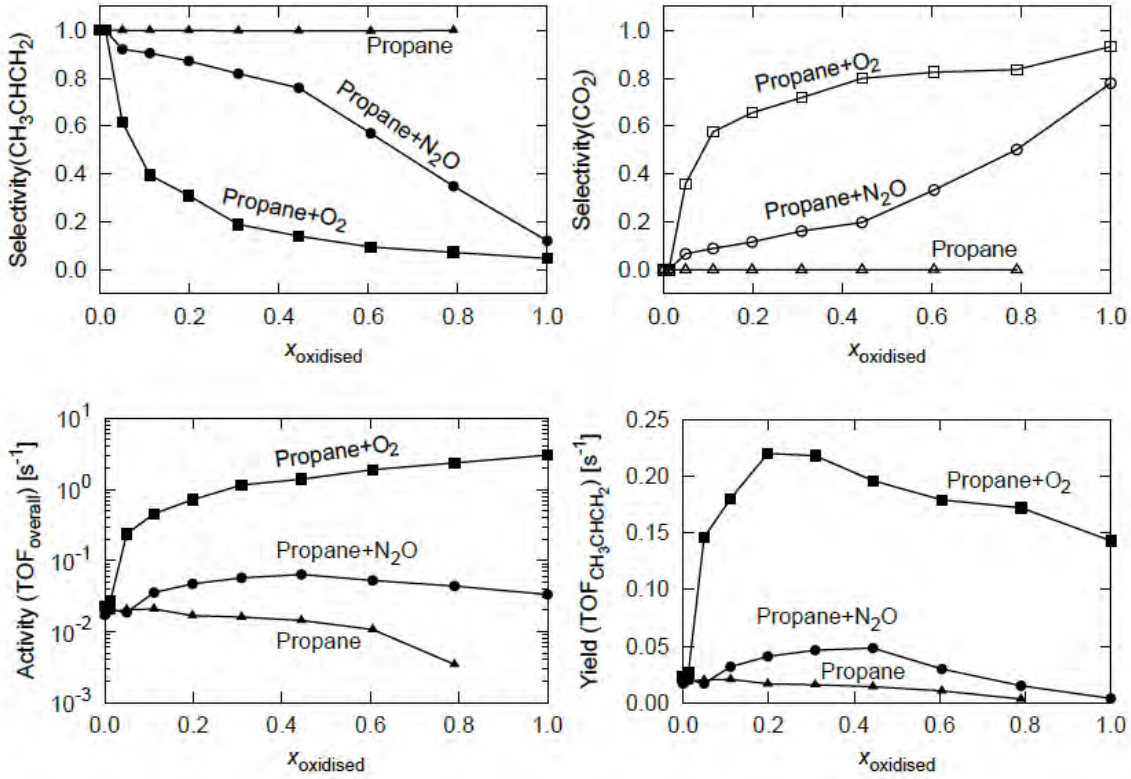

Figure 10: (top) Selectivity towards propene (left) and CO_2 (right), (bottom) Catalyst activity (left) and propene yield (right). Propane dehydrogenation is performed at $p_{CH_3CH_2CH_3} = 1.0$ bar, $p_{oxidant} = 1.0$ bar at $T = 900$ K over surfaces with a varying fraction of oxidation. Symbols shape denotes the oxidant used: ■ O_2, ● N_2O, ▲ none. Lines are the guides for an eye.

This project has received funding from the European Union's Horizon 2020 research and innovation program under grant agreement no 814671

Kinetic modelling

Methods and model (MKM):

- Solving a system of continuous differential equations
- Reaction rates are expressed as changes in surface coverage over time, computed based on reaction rate constants, reaction orders, surface coverages

$$r_n = k_f \prod_{i=1}^{I} \theta_i^{S_{i,n,f}} - k_b \prod_{j=1}^{I} \theta_j^{S_{j,n,b}}$$

- Mass balances of the surface species are sums of reaction rates times stoichiometry factors

$$\frac{d\theta_i}{dt} = R_i = \sum_{n=1}^{N} \left(-S_{i,n,f} + S_{i,n,b}\right) r_n$$

- Mass balances for gas phase species:

$$\frac{dC_i}{dt} = \frac{V\varepsilon}{F_{\text{in}}} C_{i,\text{inlet}} + C^* \frac{1-\varepsilon}{\varepsilon} R_i - \frac{V\varepsilon}{F_{\text{out}}} C_i$$

- CSTR reactor (PFR is analogously solved)
- 20 wt% catalyst loading, specific surface area 200 m^2/g, density 3.6 g/mL
- GHSV = 300 h^{-1}

Simulations in progress, results to be presented in the next GAM.

This project has received funding from the European Union's Horizon 2020 research and innovation program under grant agreement no 814671

Kinetic modelling

Butane dehydrogenation

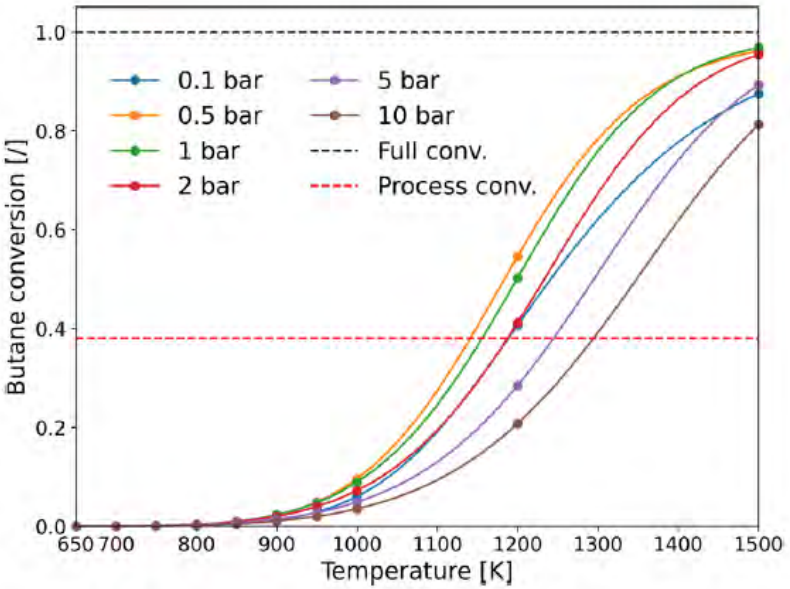

Figure 4. Butane conversion from MKM simulations at different operating conditions. The GHSV was fixed to 300 h^{-1}. The red dashed line shows the minimum conversion achieved by the CATOFIN–CATADIENE technologies.

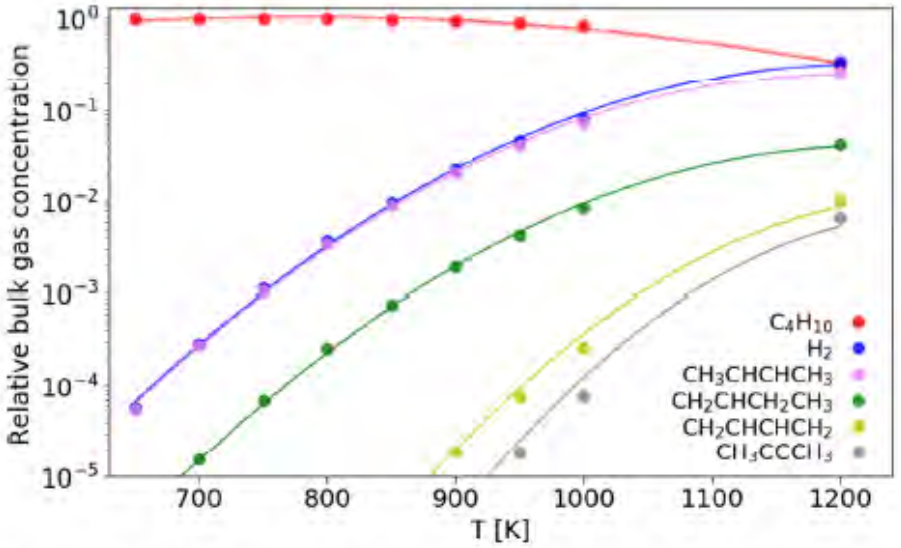

Figure 7. Bulk gas concentrations in the steady-state operation of the modelled CSTR reactor, at different temperatures. The conditions are P = 1 bar and GHSV = 300 h^{-1}.

This project has received funding from the European Union's Horizon 2020 research and innovation program under grant agreement no 814671

Kinetic modelling

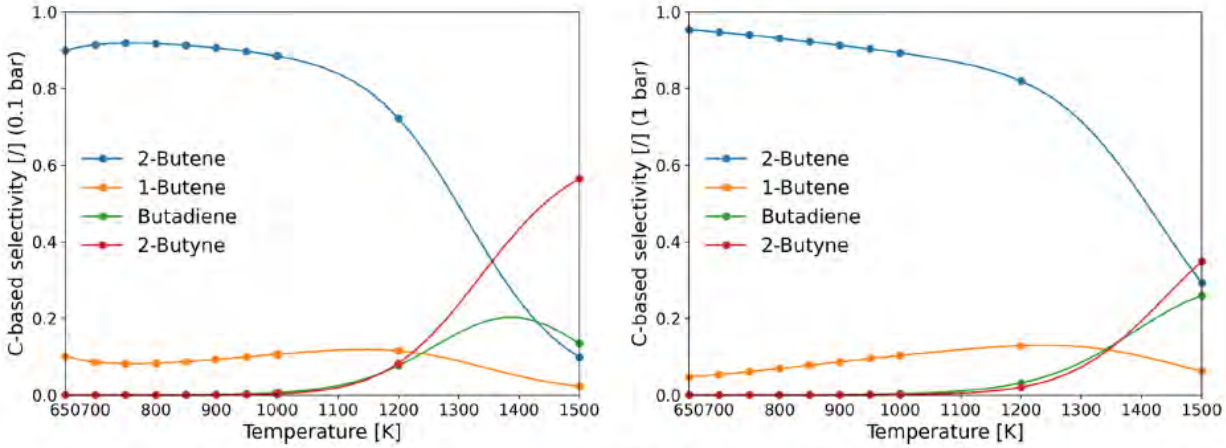

Figure 5. Selectivities to various products at different temperatures and 300 h^{-1} GHSV, at 0.1 bar (left) and 1 bar (right) pressures. The main product is 2-butene, but at higher temperatures and lower pressures, 2-butyne starts to dominate the selectivity.

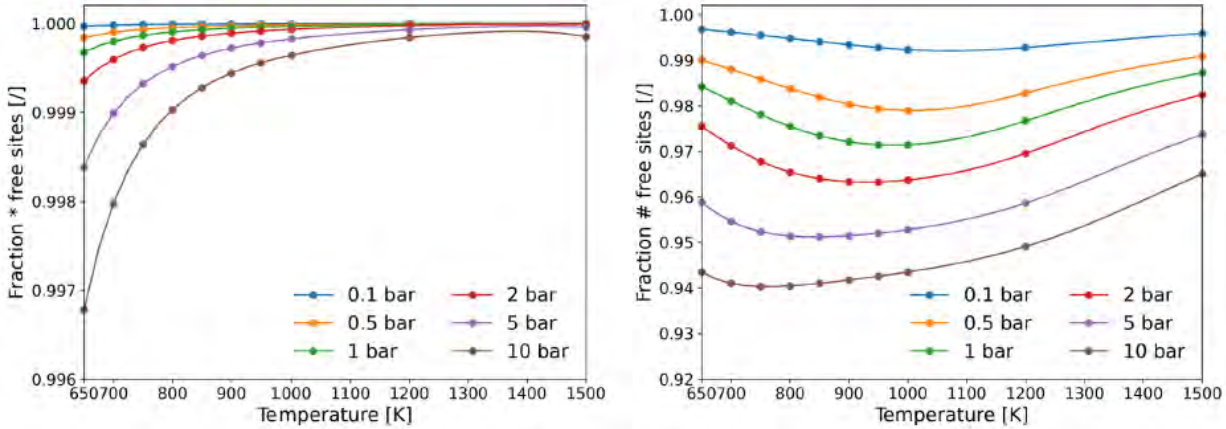

Figure 6. Relative fraction of free active sites for hydrocarbons (left) and hydrogen (right) adsorption. Surface coverage is low (maximum of ~6%) throughout various operating conditions.

This project has received funding from the European Union's Horizon 2020 research and innovation program under grant agreement no 814671

Full multi-scale

DFT obtained kinetic parameters

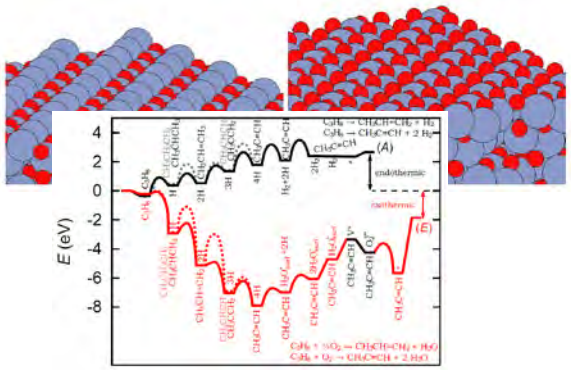

KMC reaction count and surface evolution

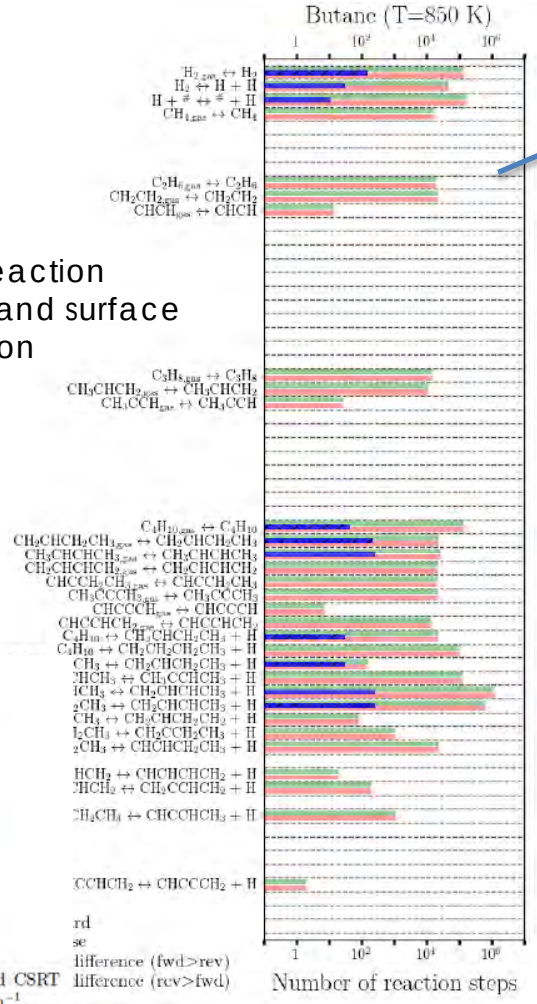

CFD

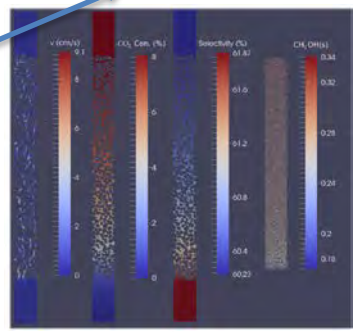

process

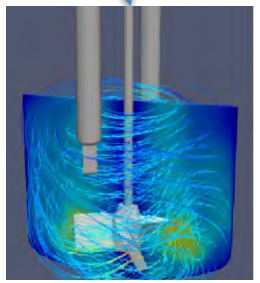

microkinetic modelling: gas phase composition

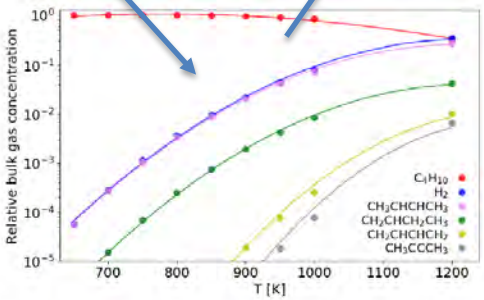

Figure 7: Bulk gas concentrations in the steady state operation of the modelled CSRT reactor, at different temperatures. The conditions are $P = 1$ bar and GHSV $= 300\,h^{-1}$.

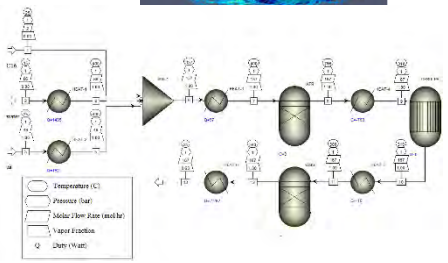

This project has received funding from the European Union's Horizon 2020 research and innovation program under grant agreement no 814671

Bifunctional Zeolite based Catalysts and Innovative process for Sustainable Hydrocarbon Transformation

BiZeolCat

Thank you for your attention

Blaz.Likozar@ki.si

This project has received funding from the European Union's Horizon 2020 research and innovation programme under grant agreement No 814671

The present publication reflects only the author's views and the European Union is not liable for any use that may be made of the information contained therein.

(*Disclosure or reproduction without prior permission of BIZEOLCAT is prohibited).*